Int. J. Electrochem. Sci., 13 **(2018)** 5709 – 5722, doi: 10.20964/2018.06.11

International Journal of
ELECTROCHEMICAL
SCIENCE
www.electrochemsci.org

Correlation between Electric Parameters and Microstructural Properties of LZ91 Mg Alloy Coated by Micro Arc Oxidation

Shun-Yi Jian[1,], Jeou-Long Lee[2], Hung-Bin Lee[3], Hung-Hua Sheu[1], Ming-Hsien Lin[1], Yu-Tong Shih[1], Chi-An Chen[1], Jun-Kai Chang[4], and Ming-Der Ger[1,**]*

[1] Department of Chemical & Materials Engineering, Chung Cheng Institute of Technology, National Defense University, Dasi, Taoyuan 335, Taiwan, ROC
[2] Department of Chemical & Materials Engineering, Lung Hwa University of Science and Technology, Tao-Yuan 330, Taiwan, ROC
[3] Department of Materials Science and Engineering, Da-Yeh University, Chang-Hua 515, Taiwan, ROC
[4] Department of Materials Science and Engineering, National Taiwan University, Taipei 106, Taiwan, ROC
[*]E-mail: ftvko@yahoo.com.tw; mingderger@gmail.com

Received: 16 January 2018 / *Accepted:* 1 April 2018 / *Published:* 10 May 2018

Micro arc oxidation (MAO) coatings are prepared on LZ91 Mg alloy at different voltages (400, 450 and 500 V). A DC, uni-polar and bi-polar power mode is used, respectively, in this work. The aim of this study is to investigate the effect of electrical parameters (power mode and voltage) on the morphology, microstructure and the corrosion behavior for LZ91 alloy. The element distribution, morphology, and corrosion resistance were studied by Electron Probe X-ray Micro-analyzer, Scanning Electron Microscope, potentiodynamic polarization in 3.5 wt.% NaCl solution and salt spray test. It is found that the increase of voltage make the coatings more porous and thicker. The applied power mode (DC, uni-polar and bi-polar modes) shows a significant influence on the coating morphology and corrosion resistance. Analysis of SST and potentiodynamic polarization technique on the samples show that the corrosion resistance of the MAO coated samples is much better than that of the bare LZ91 Mg alloy. The MAO coating prepared at 450 V under bi-polar power has smallest porosity, and hence yields best corrosion resistance on LZ91 Mg alloy.

Keywords: LZ91 Magnesium alloy; Micro arc oxidation; Corrosion resistance; Salt spray test

1. INTRODUCTION

In light of their low density and high specific strength as well as stiffness, magnesium alloys are extensively used in electric appliances and structural components. Unlike the magnesium-

aluminum alloys, the magnesium-lithium alloys are known for their excellent formability. Most of the magnesium alloys are relatively reactive and tend to suffer corrosion, especially LZ91 alloy. This difficulty is ascribed to the fact that lithium ions are completely solvable in the aqueous solution of various pHs [1-9]. Consequently, surface modifications are performed to enhance the corrosion resistance, wear resistance and paint adhesion of the base magnesium alloys. Micro arc oxidation (MAO), a novel surface engineering technology, has been considered as one of the most cost-effective and environmentally friendly ways to improve the corrosion resistance of Mg alloys [10-24].

The retarding effect of the MAO coating on the overall corrosion resistance of MAO coated Mg alloy is critically important and it depends on the level of porosity and chemical composition of the coating. It is well known that the structure and composition of the MAO coatings are controlled by substrate materials, electrical parameters and electrolyte concentration. Therefore, electrical parameters play a crucial role in obtaining the coatings with desired properties. A DC, uni-polar or bi-polar pulsed DC and AC power supplies are usually used for the MAO process. Depending on the choice of the power mode and the current or voltage parameters, coatings with different compositions, morphologies and porosity levels can be obtained. Therefore, this study investigates how the electrical parameters (power mode and voltage) influence the microstructure and the corrosion behavior of MAO coating on a LZ91 alloy.

2. EXPERIMENTAL

2.1. Preparation of specimens

Table 1. Sample codes and their respective electrical parameters for MAO treatment on LZ91 Mg alloy

Sample code	Current mode	voltage
DC 400	DC	400 V
DC 450		450 V
DC 500		500 V
UP 400	uni-polar	400 V
UP 450		450 V
UP 500		500 V
BP 400	bi-polar	400 V
BP 450		450 V
BP 500		500 V

LZ91 magnesium alloy (9.73 wt% Li, 0.84 wt% Zn, and Mg in balance) with size of 50 mm X 50 mm X 1 mm was used in this study as a substrate for MAO coating process. Prior to the MAO treatment, the surface of the plates was ground by emery paper from 800 grit up to 2000 grit, followed

by rinsing with ethanol in an ultrasonic for 10 min, washing with deionized water and drying with an air stream. The MAO coatings were formed at 400 V, 450 V and 500 V for 7 min under DC, uni-polar pulsed, and bi-polar pulsed electrical source, respectively. The process parameters during MAO process and the corresponding sample codes are listed in Table 1. The process was carried out in an electrolyte composed of 10 g/L Na_2SiO_3, 3 g/L Na_3PO_4, 1.5 g/L NaOH, and 3 g/L NaF, in which temperature was maintained at approximately 40℃. After the MAO treatment, the LZ91 plate was thoroughly rinsed with acetone in an ultrasonic for 10 min. Then, the samples were washed with deionized water and dried in cool air.

2.2. Microstructure characterization

The surface and cross-sectional morphologies of the MAO coatings were examined by scanning electron microscopy (SEM, S-3500N; HITACHI, Japan). Image J software was processed from the stored SEM images for the quantification of pore characteristics (number and average size of pores) and detection of coating defects. The Electron Probe X-ray Micro-analyzer (EPMA, JXA-8200) was utilized to identify the elements of the coating, which has been performed across the entire cross section with line scanning analysis.

2.3. Corrosion studies

To evaluate the corrosion resistance of MAO coatings, potentiodynamic polarization tests were performed for the substrate and MAO coated samples in 3.5 wt.% NaCl solution using an Autolab PGSTAT30 potentiostat-frequency analyser with GPES (General Purpose Electrochemical System) software. Potentiodynamic polarization tests were carried out in a three-electrode cell system in which a tested specimen of 1 cm^2, a platinum plate and a saturated calomel electrode were used as the working, counter and reference electrodes, respectively. After stabilization of 30 min at the open circuit potential (OCP), the potentiodynamic polarization test was performed with a scan rate of 0.5 mV/s from -300 mV to 500 mV based on the OCP. Meanwhile, the corrosion behavior of the bare and coated LZ91 alloys was also evaluated by the salt spray test (SST). The samples with a dimension of 50 mm X 50 mm X 1 mm were exposed in 5 wt.% NaCl fog for various hours. The corrosion morphologies were observed in accordance with ASTM B-117 standard. All SSTs were conducted in triplicate to confirm the reproducibility of results.

3. RESULTS AND DISCUSSION

3.1. Surface morphology of the MAO coating and compositional analyzing

Fig. 1 shows the surface morphologies of the LZ91 plate after MAO with different treatment conditions. When a DC power mode was used, an irregularly micro-structured surface was formed, as shown in Fig. 1a, b and c. It can be seen from Fig. 1 (a-c) that these surfaces were very smooth, on which many small pores were observed, which could be ascribed to the thermal stresses generated

during the growth of coating as a result of melting oxide product and the rapid solidification of magnesium oxide (MgO) [25-29]. The pore size and surface roughness both increased with increasing voltage.

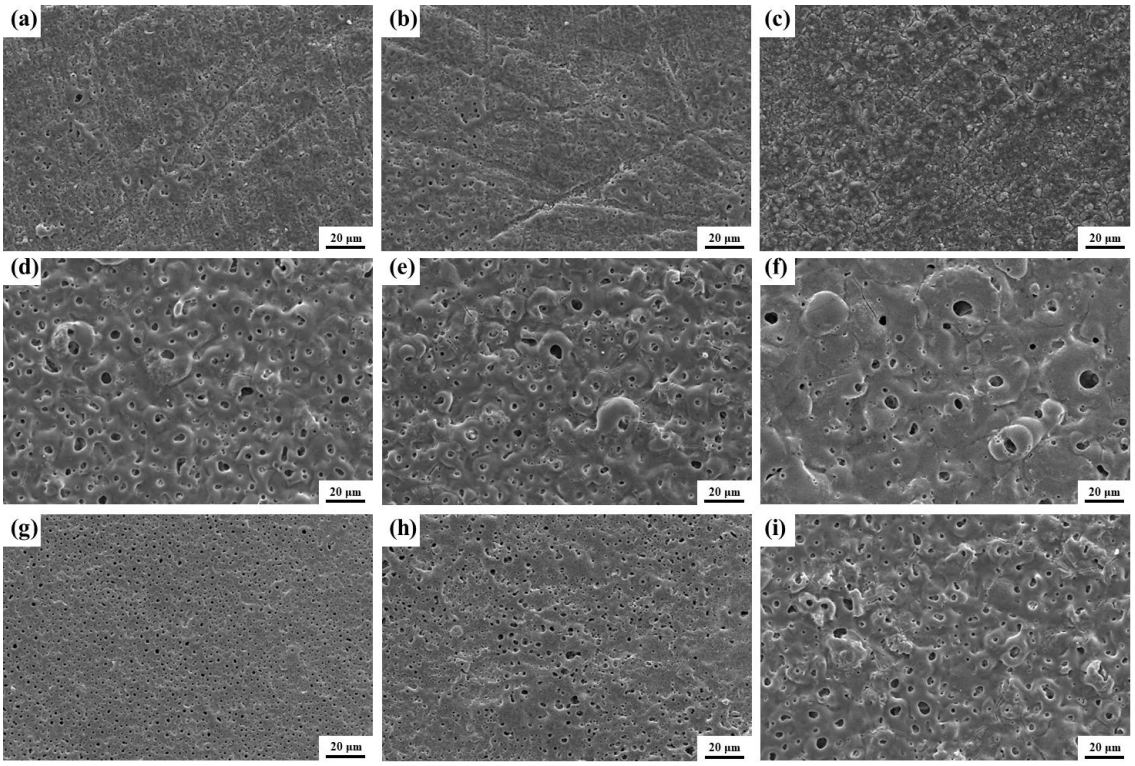

Figure 1. Surface morphology of the LZ91 alloy treated in the different electrical sources: (a-c) DC, (d-f) uni-polar and (g-i) bi-polar, respectively.

The surface morphologies of the MAO films formed under the uni-polar pulsed power mode at various voltages (400-500 V) are shown in Fig. 1 (d-f). The features of multiple micro-pores with roughly disc-like shape can be clearly seen on the coating surface. That is a well-known feature of MAO coatings. The relatively large micro-pores are produced in the center of the crater-like surface suggesting that they were produced by gas bubbles ejected from strong discharges and might penetrate deep into the coating. Hence, it causes an increase in the surface roughness. In addition, the micro-pore numbers of the MAO film decrease with increasing the applied voltage, while the average micro-pore size increases. In terms of micro arc oxidation under bi-polar pulsed mode, the evolution in surface morphology as shown in Fig. 1 (g-i) is similar to those under uni-polar pulsed mode. However, the MAO coating produced by using the bi-polar pulsed mode was found to improve the coating quality compared with the uni-polar current mode, in terms of surface morphology where the pore size was reduced significantly and the surface became smoother, which might influence the corrosion behavior.

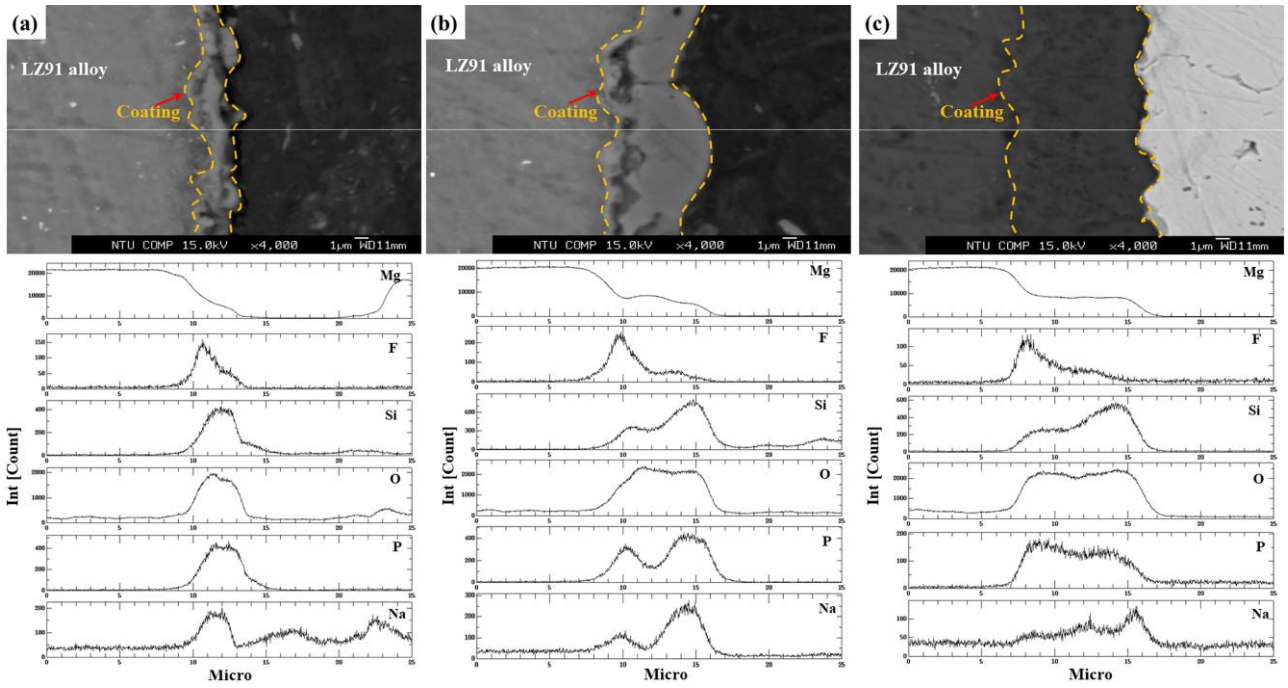

Figure 2. Cross-sectional composition of the coatings on LZ91 Mg alloy determined by EPMA.

Distribution of main chemical elements across MAO coatings on DC 450, UP 450 and BP 450 are investigated using Electron Probe X-ray Micro-analyzer (EPMA) method. EPMA analysis results are shown in Fig. 2. During MAO treatment, the Mg^{2+} ions are derived at the anode-electrolyte interface and the dissociation of ions such as F^{-}, $SiO_3^{2-}$and PO_4^{3-} ions in the bath might be incorporated into the oxide coating during micro arc oxidation. Therefore, the MgO, MgF_2, Mg_2SiO_4 and $Mg_3(PO_4)_2$ are the main chemical compounds that exist in the MAO coating [30-31]. It can also be found that Si and P elements mainly distribute at the outer region within the coating, while F prefers to distribute at the inner region. The element distribution result that the Si content is higher in the outer region than that in the inner one and F content in the inner region is higher than that in the outer region is in good agreement with a previous work [32]. The fact that enrichment of F nears to the coating/substrate interface suggests the formation of MgF_2 during the initial stages of MAO process.

3.2. Corrosion Properties of the Coatings

MAO coatings contain unavoidable micro-pores, which might deteriorate the corrosion resistance of the coatings. Barik investigated the corrosion property of MAO coatings, and demonstrated that unsealed MAO coating let penetration of the corrosive medium through the micro-pores in the coating [33]. In addition, the results from literatures concerning the corrosion protection effect of MAO coating on magnesium alloys showed that the corrosion resistance of MAO coatings was not directly related to the coating thickness [33-35]. In order to examine the corrosion behavior of the coatings, the potentiodynamic polarization tests and salt spray tests were carried out. The Tafel extrapolation of polarization curves is widely used for the evaluation of the corrosion of magnesium alloys, because it is simple and fast. In this study, polarization curves of the bare and coated LZ91

plates in 3.5 wt.% NaCl solution are illustrated in Fig. 3. The electrochemical values of the corrosion potential (E_{corr}), the corrosion current density (i_{corr}) and anodic/cathodic Tafel slopes β_a and β_c extracted from the polarization curves are listed in Table 2.

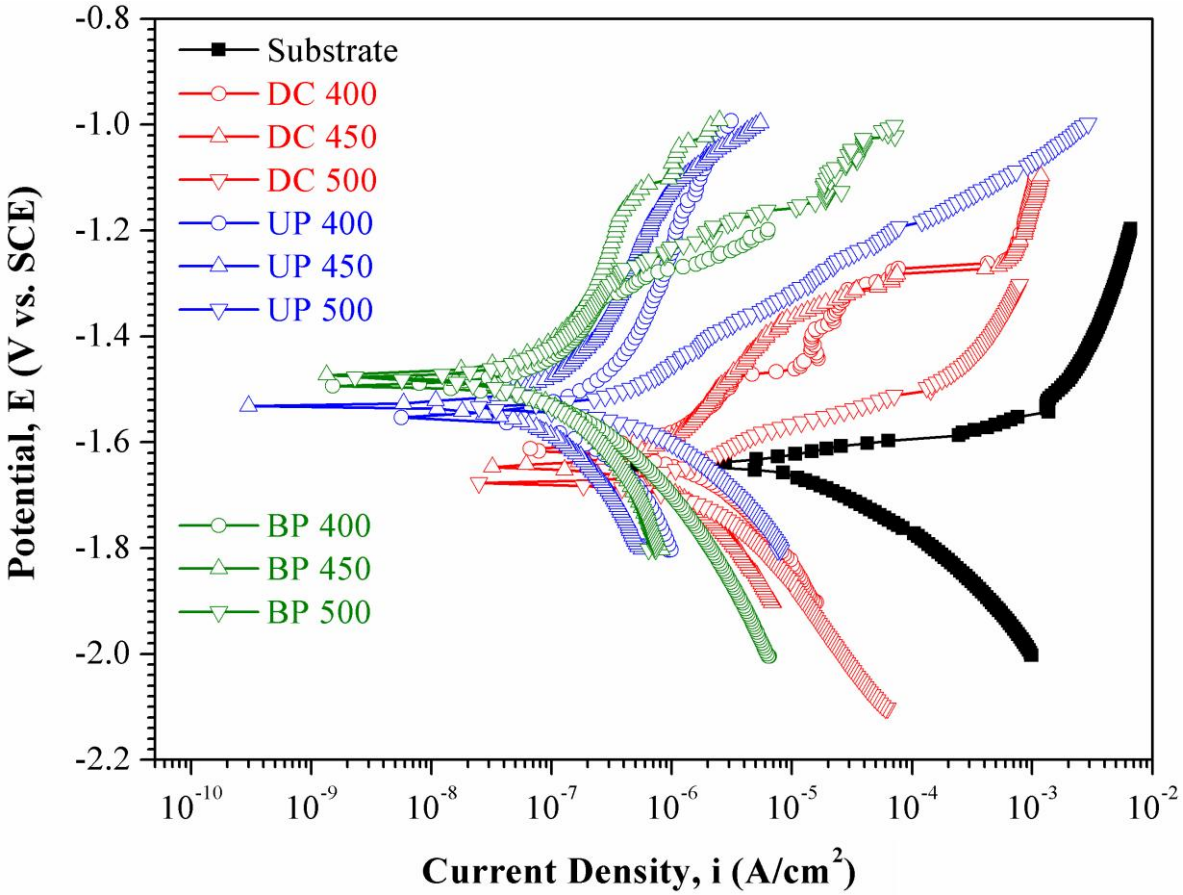

Figure 3. Potentiodynamic polarization curves of bare LZ91 and the MAO coated LZ91 samples in 3.5 wt.% NaCl solution.

Table 2. Results of potentiodynamic polarization tests of bare LZ91 and the MAO coated LZ91 Mg alloy in 3.5 wt.% NaCl solution.

Sample	E_{corr} (V vs SCE)	I_{corr} (A/cm^2)	β_a (V/decade)	β_c (V/decade)
Substrate	-1.75	3.71×10^{-5}	0.036	-0.159
DC 400	-1.58	1.51×10^{-6}	0.222	-0.096
DC 450	-1.64	1.03×10^{-6}	0.225	-0.088
DC 500	-1.67	2.15×10^{-6}	0.111	-0.117
UP 400	-1.58	1.01×10^{-7}	0.373	-0.089
UP 450	-1.53	3.45×10^{-7}	0.378	-0.071
UP 500	-1.54	7.58×10^{-7}	0.122	-0.134
BP 400	-1.48	1.41×10^{-7}	0.310	-0.111
BP 450	-1.46	5.04×10^{-8}	0.387	-0.069
BP 500	-1.47	3.80×10^{-7}	0.323	-0.075

The results shown in Table 2 demonstrate that the bare LZ91 has a lowest E_{corr} and highest i_{corr}, indicating that it has a highest corrosion rate. Compared to the bare LZ91, all MAO-coated samples exhibited a lower corrosion current density and a higher corrosion potential. It indicates that MAO coatings significantly improve the corrosion resistance of the LZ91 alloy.

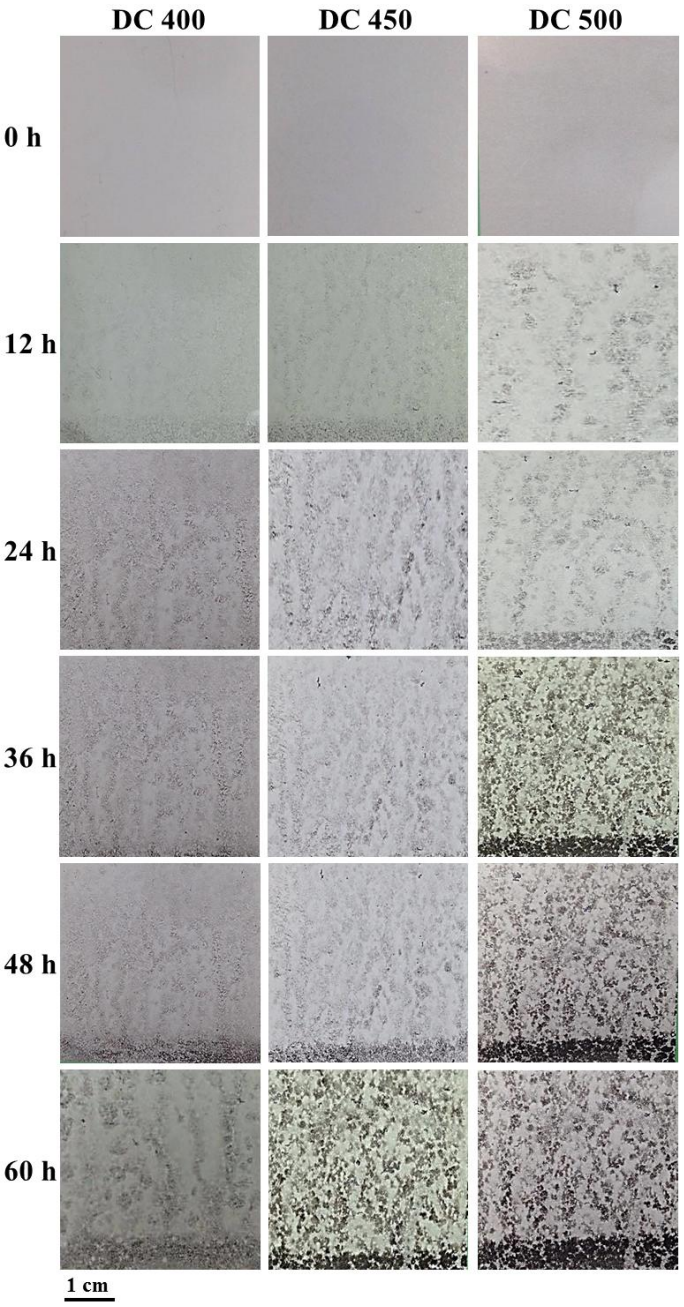

Figure 4. Optical images of the MAO coated LZ91 plate prepared under DC power mode after 60 h SST.

The ranking for the i_{corr} values obtained in the potentiodynamic polarization tests for various MAO coatings was LZ91 uncoated < MAO coated samples prepared under DC < MAO coated samples prepared under uni-polar pulsed power < MAO coated samples prepared under bi-polar pulsed

power. In particular, the sample BP 450 had the lowest corrosion current density, which is about three orders of magnitude lower than that of the substrate, indicating this coating had best corrosion resistance among tested MAO coatings.

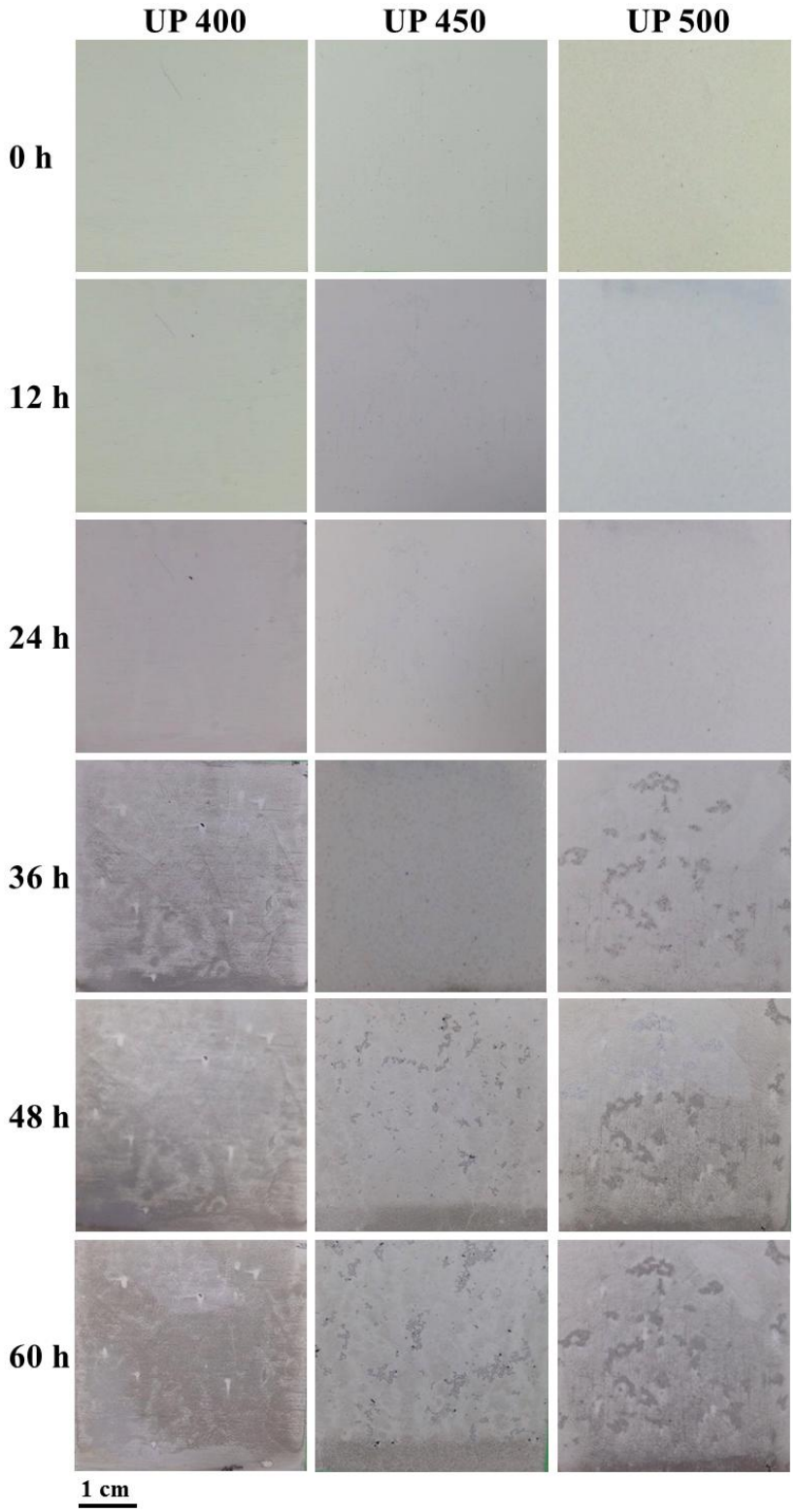

Figure 5. Optical images of the MAO coated LZ91 plate for uni-polar pulsed electrical source after 60 h SST.

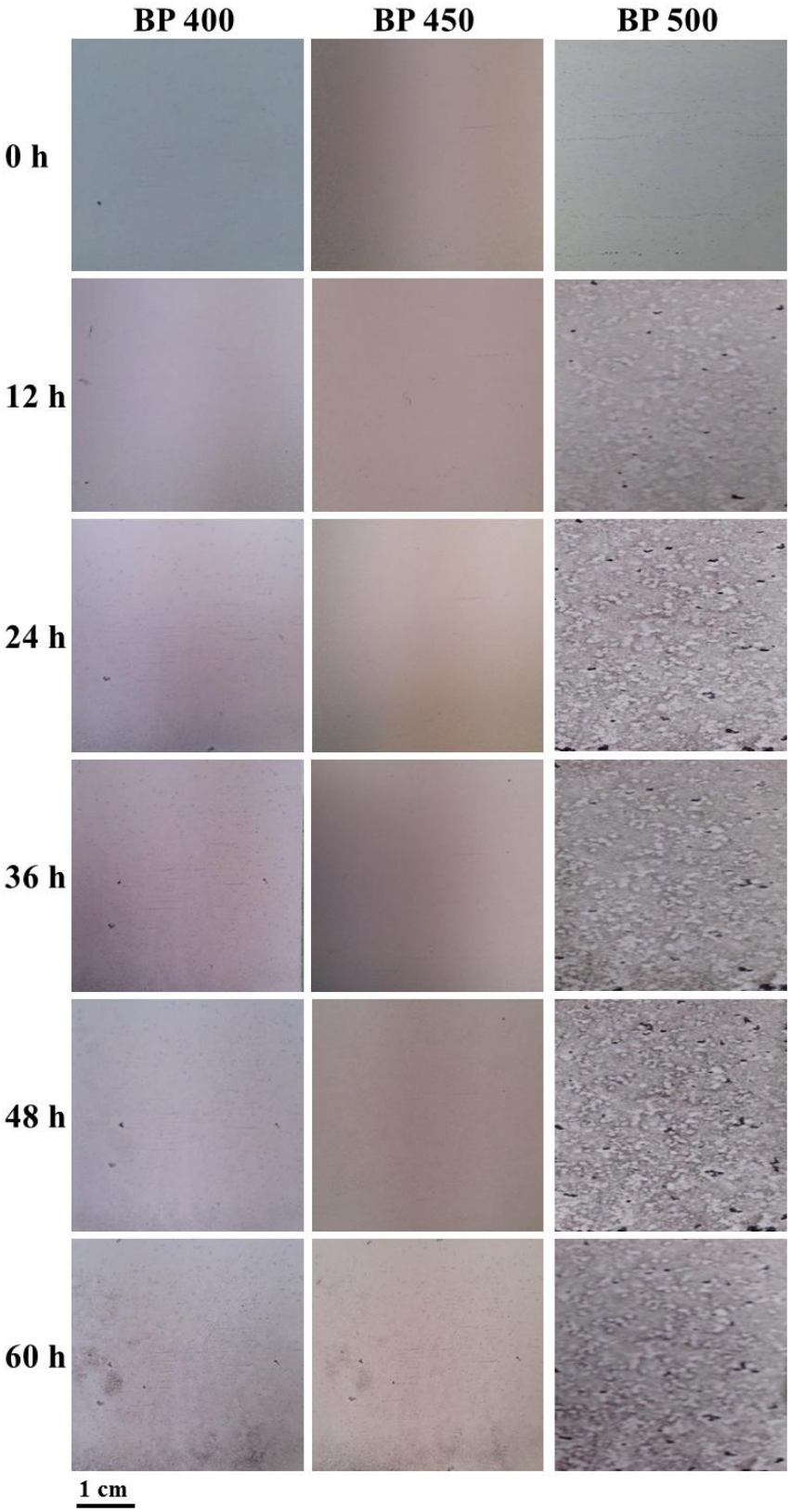

Figure 6. Optical images of the MAO coated LZ91 plate prepared under bi-polar pulsed power mode after 60 h SST.

In addition, the anodic polarization branch exhibited a passivation behavior instead of the Tafel behavior, the i_{corr} was acquired by an extrapolation of the β_c back to E_{corr}, in which β_c was obtained from the cathodic polarization branch at -50 mV vs. the E_{corr}. The β_a is also calculated from the anodic polarization curve at +50 mV vs. the E_{corr}. For comparison, the curves of the samples coated with the DC power show that there are limited improve on resistance against anodic polarization. The current increases quite rapidly after passing the free corrosion potential. It indicates that the MAO film appears as pitting corrosion and surface defects (micro-crack) on the MAO film due to the corrosion products dissolving into test solution. In other words, the sample coated with the DC electrical source is not effective to obstruct the aggressive attack of chloride ions (Cl^-) to transfer through the outer porous layer and reach the inner barrier layer of MAO layer slowly with increasing anodic potential during the polarization. Thus, its corrosion resistance is inferior to those MAO coatings prepared under pulsed power modes.

The corrosion behaviors of MAO coated LZ91 plates were evaluated by salt spray test again. The surface appearances of the three sets of samples produced under DC, uni-polar pulsed, and bi-polar pulsed power during the 60 hours SST are shown in Figs. 4-6, respectively. Fig. 4 shows that a large part of the corroded area with the occurrence of filiform corrosion and the presence of abundant corrosion cavities can be clearly observed for the samples coated with the DC power. The series of photographs in Fig. 5 show that the presence of many small-scale attack sign for these samples coated with the uni-polar pulsed power. The corrosion area of the samples BP 400 and BP 450 is relatively small, as shown in Fig. 6. But for the samples BP 500, noticeable corroded areas which the color became dark can be seen on the surface. According to the results of salt spray tests the best corrosion performance was displayed by the sample BP 450, which is consistent with the results obtained from the potentiodynamic polarization tests.

3.3. Porosity and pore size analysis

Table 3. The average porosities of various MAO coated LZ91 Mg alloy, together with the micro-pores size and the corrosion area fraction (%) after 60 h SST.

Sample	Number of Spots					Mean Spots Diameter (μm)	Area Percent of spots (% of total)	Corrosion area fraction (%) after 60 h SST
	Spots size (μm)							
	＜1	1~5	5~10	＞10	total			
DC 400	$9.7x10^2$ ($\pm 1.0x10^1$)	$9.8x10^1$ ($\pm 1.0x10^1$)	—	—	$1.0x10^3$ ($\pm 7.5x10^2$)	1.13	48.8	42
DC 450	$6.8x10^2$ ($\pm 1.0x10^1$)	$1.3x10^2$ ($\pm 1.0x10^1$)	—	—	$8.2x10^2$ ($\pm 1.0x10^1$)	1.23	47.9	58
DC 500	$4.0x10^2$ ($\pm 1.0x10^1$)	$2.8x10^2$ ($\pm 1.0x10^1$)	—	—	$7.0x10^2$ ($\pm 1.0x10^1$)	1.62	46.2	63

UP 400	20 (±3.0)	$1.2x10^2$ ($±1.0x10^1$)	4.0 (±1.0)	—	$1.5x10^2$ ($±1.0x10^1$)	2.43	29.0	28
UP 450	40 (±5.0)	$1.5x10^2$ ($±1.0x10^1$)	10 (±2.0)	—	$2.0x10^2$ ($±1.0x10^1$)	2.45	25.3	20
UP 500	10 (±2.0)	$4.6x10^1$ ($±1.0x10^1$)	28 (±3.0)	2.0 (±1.0)	$9.0x10^1$ ($±1.0x10^1$)	4.06	19.7	38
BP 400	60 (±8)	$1.8x10^2$ ($±1.0x10^1$)	—	—	$2.5x10^2$ ($±1.0x10^1$)	2.12	20.1	5
BP 450	40 (±3.0)	$1.3x10^2$ ($±1.0x10^1$)	5.0 (±1.0)	—	$1.8x10^2$ ($±1.0x10^1$)	2.30	15.1	3
BP 500	35 (±5.0)	$6.0x10^1$ ($±1.0x10^1$)	25 (±2.0)	—	$1.3x10^2$ ($±1.0x10^1$)	3.07	22.3	38

The SEM images shown in Fig. 1 were image-processed by Image-J software for porosity analysis. The averaged porosities determined from on SEM images for a typical surface area of 125 x 185 μm^2, are listed in Table 3, together with the micro-pores size and the corrosion area fraction (%) after 60 h SST. Hussein investigated the micro-pores size and reported that the micro-pores varied in size from very small diameters (<1μm) through medium size (few μm) to large cavities (>10 μm) [26-27].

As can be seen from Table 3, the MAO samples produced under DC power exhibit that the diameter of all pores is smaller than 5 μm, but the level of porosity is quite high (> 46%). Larger pore size, less pore number and smaller porosity are seen for samples prepared using uni-polar mode compared to those prepared using the DC mode. The LZ91 specimen MAO coated under bi-polar pulsed mode show a largest average pore size and a lowest porosity around 20 % among all the samples. Generally, the micro-pores number as well as the porosity decreases and mean diameter increases as the voltage increases. However, the porosity increases from 15.1% to 23.2% as the voltage of bi-polar pulsed mode increases from 450 V to 500 V. Compared to the DC sample, the pulsed sample has relatively less pores in the same area. Changing the current mode produces changes in the breakdown voltage and discharge intensity and density. For MAO treatment at the same voltage, the pulsed mode provides a larger current pulse in the working range compared to the DC mode, thus enabling the creation of shorter but more micro discharge events, which results in increase the growth rate and formation of a thicker layer. On the other hand, in the range of a negative pulse or current turning off, sparks disappear and locally melted coatings are rapidly quenched by the electrolyte resulting in porous structure of coatings. Moreover, the cathodic component in the bi-polar mode might lead to the dissolution of some oxide phase on the coating surface [36], which increased the conductivity of the electrolyte. Increasing the electrolyte conductivity leads to an enhancement of the discharge intensity, thus discharge channels become larger [37]. As a result, a coating with relatively great micro-pores is formed.

Fig. 7 shows the effect of mean micro-pores diameter, area percent of defects on the corrosion resistance based on the results of SST. It is obvious that there are three factors having a significant effect on the corrosion properties of the MAO coatings. These factors are porosity level and pores size. Compared to the other samples, the sample prepared under bi-polar mode has a less micro-pores and porosity are primarily responsible for the better corrosion resistance.

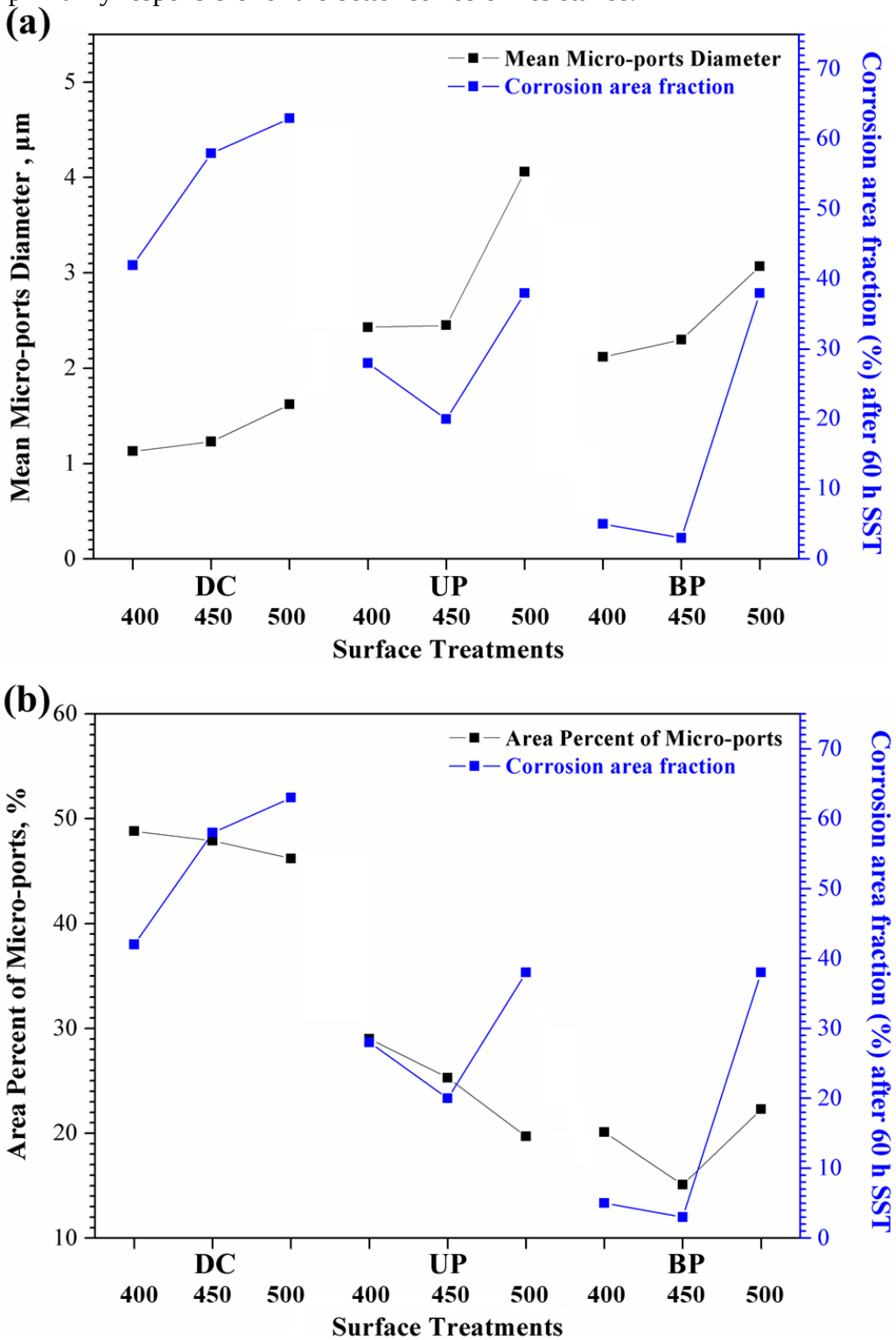

Figure 7. The effect of (a) mean micro-ports diameter and (b) area percent of defects on the corrosion resistance of MAO coating after 60 h SST analyses.

4. CONCLUSIONS

The different power modes (DC, uni-polar and bi-polar) and voltages were used in the MAO treatment of LZ91 magnesium alloy. Applying different electrical parameters exerts a remarkable influence on surface morphologies (pore size and level of porosity) of the MAO coatings. In general, the average pore size of coating increase and the level of porosity decreases as the voltage increases. MAO coated samples prepared under DC mode contained more porosity as compared to other samples prepared under different modes. Therefore, the coatings produced under DC mode had the worst corrosion resistance. The properties of the electrical discharges themselves in the bi-polar pulsed electrical mode differ from those of the uni-polar one. On the contrary, applying the bi-polar pulsed power mode with a cathode component changes the surface morphology of the MAO coatings, resulting in the formation of a more compact coating with less porosity, which enhances the corrosion resistance.

ACKNOWLEDGEMENT
This study was financially supported by the Ministry of Science and Technology of Taiwan, Republic of China, under Grant No. MOST 106-2221-E-606-013-MY3.

References

1. J. E. Gray, B. Luan, *J. Alloys Comp*., 336 (2002) 88.
2. Y. Kojima, *Mater. Trans*., 42 (2001) 1154.
3. S. Kamado, T. Ashie, Y. Ohshima, Y. Komija, *Mater. Sci. Forum*., 350 (2000) 55.
4. S. Ono, Y. Suzuki, H. Asoh, N. Hanzawa, M. Hyakutake, *Mater. Sci. Forum*., 426 (2003) 581.
5. S. Dong, T. Imai, S. W. Lim, N. Kanetake, N. Saito, I. Shigematsu, *Mater. Manuf. Processes*, 23 (2008) 336.
6. K. Funatani, *Surf. Coat. Tech*., 264 (2000) 133.
7. H. Takuda, S. Kikuchi, N. Yoshida, H. Okahara, *Mater. Trans*., 44(11) (2003) 2266.
8. C. C. Hsu, J. Y. Wang, and S. Lee, *Mater. Trans*., 49(11) (2008) 2728.
9. Z. Yang, J. P. Li, J. X. Zhang, G. W. Lorimer, J. Robson, *Acta Metall. Sin*., 21(5) (2008) 313.
10. A. L. Yerokhin, A. Leyland, A. Matthews, *Appl. Surf. Sci*., 200 (2002) 172.
11. H. P. Duan, C. W. Yan, F. H. Wang, *Electrochim. Acta*, 52 (2007) 3785.
12. L. L. Shi, Y. Xu, K. Li, Z. P. Yao, S. Wu, *Curr. Appl. Phys*., 10 (2010) 719.
13. Z. Z. Qiu, R. Wang, X. H. Wu, Y. S. Zhang, *Int. J. Electrochem. Sci*., 8 (2013) 1957.
14. S. V. Gnedenkov, O. A. Khrisanfova, A. G. Zavidnaya, S. L. Sinebryukhov, V. S. Egorkin, M. V. Nistratova, A. Yerokhin, A. Matthews, *Surf. Coat. Technol*., 204 (2010) 2316.
15. C. E. Barchiche, D. Veys-Renaux, E. Rocca, *Surf. Coat. Technol*., 205 (2011) 4243.
16. I. J. Hwang , D.Y. Hwang , Y.G. Ko, D.H. Shin, *Surf. Coat. Technol*., 206 (2012) 3360.
17. Z. J. Li, Y. A. Yi, X. Y. Jing, *J. Alloys Compd*., 541 (2012) 380.
18. G. K. Young, S. L. Eung, H. S. Dong, *J. Alloys Compd*., 586 (2014) 357.
19. D. Veys-Renaux, C.-E. Barchiche, E. Rocca, *Surf. Coat. Technol*., 251 (2014) 232.
20. H. Gao, M. Zhang, X. Yang, P. Huanga, K. Xu, *Appl. Surf. Sci*., 314 (2014) 447.
21. X. J. Cui, C. H. Liu, R. S. Yang, M. T. Li, X. Z. Lin, *Surf. Coat. Technol*., 269 (2015) 228.
22. Y. Si, Z. Xiong, X. Zheng, M. Li, Q. Yang, *Int. J. Electrochem. Sci*., 11 (2016) 3261.
23. H. Tang, Y. Gao, *J. Alloys Compd*., 688 (2016) 699.
24. Y. Xia, Z. Zhu, L. Chang, J. Zhang, F. Cao, J. Zhang, *Int. J. Electrochem. Sci*., 12 (2017) 2145.

25. S. Y. Jian, J. L. Lee, H. B. Lee, H. H. Sheu, C, Y. Ou, M. D. Ger, *J. Taiwan. Inst. Chem. Eng*., 68 (2016) 496.
26. R. O. Hussein, X. Nie, D. O. Northwood, A. Yerokhin, A. Matthews, *J. Phys. D: Appl. Phys*., 43 (2010) 105203.
27. S. J. Lee, L. H. T. Do, J. L. Lee, H. C. Peng, *Int. J. Electrochem. Sci*., 12 (2017) 11256.
28. J. A. Curran, T. W. Clyne, *Acta Mater*., 54 (2006) 1985.
29. R. O. Hussein, D. O. Northwood, X. Nie, *J. Alloys Compd*., 541 (2012) 41.
30. J. Liang, J. Tian, H. Liu, J. Zhou, W. Liu, T. Xu, *Surf. Coat. Technol*., 199 (2005) 121.
31. L. L. Liu, P. X. Yang, C. N. Su, H. F. Guo, M. Z An, *Int. J. Electrochem. Sci*., 8 (2013) 6077.
32. S.V. Gnedenkov, O.A. Khrisanfova, A.G. Zavidnaya, S.L. Sinebryukhov, V.S. Egorkin, M.V. Nistratova, *Surf. Coat. Technol*., 204 (2010) 2316.
33. R. C. Barik, J. A. Wharton, R. J. K. Wood, K. R. Stokes, R. L. Jones, *Surf. Coat. Technol.*, 199 (2005) 158.
34. C. E. Barchiche, E. Rocca, C. Juers, J. Hazan, J. Steinmetz, *Electrochim. Acta*, 53 (2007) 417.
35. A. S. Gnedenkov, S. L. Sinebryukhov, D. V. Mashtalyar, S. V. Gnedenkov, *Surf. Coat. Technol.*, 225 (2013) 112.
36. A.L. Yerokhin, X. Nie, A. Leyland, A. Matthews, *Surf. Coat. Technol*., 130 (2000) 195.
37. V. Ezhilselvi, Nithin J, J.N.Balaraju, S.Subramanian, *Surf. Coat. Technol*., 288 (2016) 221.